Hydrogen trapping of carbides during high temperature gaseous hydrogenation

Liese Vandewalle[1], Tom Depover[1]*, Kim Verbeken[1]*

[1] Ghent University, Department of Materials, Textiles and Chemical Engineering, Sustainable Materials Science, Technologiepark-Zwijnaarde 46, B-9052 Ghent, Belgium
Liese.Vandewalle@UGent.be
*Tom.Depover@UGent.be (+3293310433)
*Kim.Verbeken@UGent.be (+3293310453)
*corresponding authors

Abstract

This study evaluates the hydrogen absorption and trapping in carbide containing steels from a very low hydrogen partial pressure atmosphere at elevated temperatures. Two generic titanium-containing Fe-C steels, differing in carbon and titanium content, are studied. The steels are subjected to a quench and temper treatment, where tempering is performed in a dilute hydrogen gas atmosphere. Detailed microstructural analysis via SEM and TEM together with characterization via thermal desorption spectroscopy and hot extraction are performed to analyze the hydrogen trapping ability of the different types of carbides.

A significant amount of hydrogen is introduced in the Fe-C-Ti alloys during tempering. Moreover, the hydrogen appears to be strongly trapped. This could be related to trapping at the carbon-vacancies inside the TiC, and more specifically the large undissolved carbides. The binding energy is estimated to range between 80 kJ/mol and 90 kJ/mol and appears to be independent of the undissolved carbide size.

Keywords: carbides, hydrogen trapping, thermal desorption spectroscopy, gaseous charging

Introduction

It is well-known that the presence of hydrogen in steel may cause strong degradation of the material's mechanical properties, leading to so called hydrogen embrittlement (HE)[1, 2]. As a consequence, premature failure may occur, endangering the safety and reliability of the metal infrastructure. Since hydrogen can be introduced in the material during production as well as in service, the HE of steels proposes a serious issue for many engineering sectors. Especially, the shift towards hydrogen economy has considerably increased the need for improved understanding of the HE behavior of currently used materials in infrastructure, together with the development of new materials with a high resistance against HE. The use of hydrogen gas as an energy carrier will be part of the solution for carbon neutral production. However, due to the easy penetration and diffusion of hydrogen in steels, safe storage and transportation of the hydrogen gas (via retrofitting of the existing pipeline network) remain a crucial concern [3-11]. Moreover, the use of hydrogen as a fuel for vehicles also require the development of materials with both high strength and high HE resistance [12, 13].Upon hydrogen entry in the metal, the hydrogen atoms may diffuse towards critical points in the microstructure and assist there in crack formation and growth. Consequently, a possible strategy to enhance a steel's resistance against HE is the introduction of well-designed traps for hydrogen in the steel microstructure. In this perspective, titanium carbides have been reported to be of large interest, since they are readily added to steels for their significant strengthening effect due to secondary hardening [14-16] and, moreover, can have a beneficial effect on the resistance against hydrogen embrittlement [16-18]. However, the

beneficial effect on the HE resistance of the carbides strongly depends on their hydrogen trapping ability [16, 19-21].

Consequently, understanding the interaction of hydrogen with these carbides is of major importance. Generally, trapping sites associated to carbides can be related to the elastic strain field surrounding the carbide, the carbide/matrix interface and the interior of the carbide. One of the first studies on the H trapping of titanium carbides was performed by Pressouyre and Bernstein [22] by use of the hydrogen permeation technique as developed by Devanathan and Stachurski [23]. The materials used in their study were reported to consist out of a ferritic matrix, incoherent titanium carbides (TiC) and substitutional titanium (Ti) atoms and, in some cases, coherent carbides. They observed a strong delay of the permeation curve, for both the first and the second transient upon addition of Ti. Consequently, the presence of Ti resulted in the introduction of hydrogen trapping sites in the microstructure. Moreover, for all alloys the second transient was faster than the first, indicating that irreversible traps were present in the materials which got filled during the first transient but no longer affected the second transient. It must be noted however that this observation was also made for the pure iron reference. They suggested that the Ti atoms in solid solution acted as reversible traps whereas the TiC, and especially the large incoherent ones, provided irreversible trapping sites. The latter assumption was based on the microautoradiography results from Asaoka [24], showing that precipitate-matrix interface of spherical TiC can act as strong trapping sites. While, the Ti atoms were considered to attract hydrogen based on the consideration of chemical and electrical binding forces. Via analysis of the permeation transients they found a binding energy for hydrogen to the substitutional Ti atoms ranging between 21 kJ/mol and 26 kJ/mol and a binding energy to the TiC of 95 kJ/mol. Later studies on the interaction of hydrogen with titanium carbides were performed both by permeation and thermal analysis but led to contradictory results. Stevens and Bernstein [25] evaluated the hydrogen trapping behavior of a Ti micro-alloyed steel as a function of the ageing temperature by use of the electrochemical permeation. They found that precipitation of fine coherent TiC resulted in the introduction of irreversible traps but coarsening decreased the irreversible nature of the traps, indicating that the trapping strength was reduced with decreasing degree of coherency. In addition, based on combined electrochemical permeation experiments and microstructural analysis Valentini et al. [26] identified the fine coherent Ti(C,N) as irreversible trapping sites. On the other hand, Lee and Lee [27] used thermal desorption spectroscopy (TDS) to study the hydrogen trapping by TiC inclusions after gaseous charging under a relatively high hydrogen pressure of 0.1 MPa and at elevated temperatures (around 400°C). No information was given on the type of carbides but based on the isothermal holding for 24h at 700°C together with the absence of an austenitization step, the TiC can be assumed to have an incoherent interface. Analysis of the TDS spectra resulted in a high activation energy for de-trapping, indicating their irreversible nature. While the dependency of the hydrogen content on charging temperature indicated a rather low binding energy, i.e. 28 kJ/mol, of hydrogen to the TiC. In a later study, Lee and Lee [28] evaluated the effect of the TiC/matrix interface character on the hydrogen trapping. Again hydrogen charging was carried out under a 0.1 MPa H_2 containing environment at 400°C and trapping analysis was done by TDS. They found that both the incoherent carbides as the semi-coherent carbides could provide trapping sites but the trapping strength was smaller for the semi-coherent ones.

Thorough investigations performed by Wei and Tsuzaki [29-32] helped in clarifying this discrepancy. They showed that while incoherent carbides could indeed act as irreversible trapping sites, they could only be filled at elevated temperatures and hence not by electrochemical charging at room temperature. In their studies, the hydrogen at elevated temperatures was provided by the water-vapor oxidation during tempering in a non-protective atmosphere. Moreover, they showed that the hydrogen was trapped inside the bulk of these carbides rather than at the incoherent interface.

Considering the TiC crystal structure, they proposed the carbon-vacancies inside TiC were responsible for the strong trapping. Consequently, the necessity for elevated temperatures was related to a high barrier for hydrogen migration inside the carbides. On the other hand, coherent and semi-coherent carbides were able to trap hydrogen relatively strongly after electrochemical charging but not at elevated temperatures. In this case, the trapping sites were related to the (semi-)coherent interface and more specifically the misfit dislocation cores. The elastic strain field was considered to be only very weakly attracting hydrogen and hence did not contribute to the trapping. As these trapping sites were filled after electrochemical charging no high energy barrier to enter the trapping sites was expected.

Di Stefano et al. [33] used density functional theory (DFT) calculations to study the hydrogen trapping by TiC. They found that hydrogen binds very strongly to carbon-vacancies inside the TiC, with binding energies of around 105 kJ/mol, while misfit dislocations at the semi-coherent TiC/Fe interface provided less strong binding to hydrogen (with a binding energy of around 44 kJ/mol). The incoherent interface and perfectly coherent interface were only weakly attractive for hydrogen. Moreover, they reported an extremely high energy barrier for hydrogen to enter the TiC. Thus, these results were in perfect agreement with the findings of Wei and Tsuzaki. Since then multiple studies have been performed on the hydrogen trapping behavior of TiC after electrochemical charging [16, 34-38]. These studies showed that fine precipitated carbides could trap high amounts of hydrogen at their (semi-) coherent interfaces with fairly strong activation energies ranging from 40 kJ/mol to 60 kJ/mol. Depover et al. [16] even reported even higher activation energies of 70 and 117 kJ/mol which they related to the semi-coherent carbide/matrix interface. Moreover, the trapping capacity appeared to depend on the carbide sizes. Depover et al. [16] reported the carbides smaller than 30 nm to have the highest trapping capacity, while carbides with a size of 70 nm were unable to trap due to the incoherent character of their interface. More in-depth information on the trapping by TiC after electrochemical charging was obtained via a model-based evaluation of TDS spectra as was done by Drexler et al. [34, 39] For this purpose, they developed a trap-diffusion integrated finite element model which allowed a more in-depth interpretation of the experimental spectra obtained in [3]. As such they were able to not only obtain trap binding energies but also trap densities. Correlating this information to experimental microstructural characterization and atomistic simulation data on binding energies, four different trapping sites linked to the precipitated TiC could be identified. An overview of their findings is given in Table 1. Again the broad semi-coherent interface was found to be the most important for trapping, and more specifically the carbon-vacancies at the interfaces. However, they also reported very strong trapping (with binding energy of around 103kJ/mol) by carbon-vacancies inside small titanium carbides. Atom probe tomography (APT) studies [35, 40-42] were able to visualize the hydrogen, or actually deuterium (D) atoms trapped at the carbides. In this case the needle specimen were cathodically charged using D_2O. Takahashi et al. [35] observed a homogeneous segregation of D atoms at the broad interface of larger (i.e. semi-coherent) precipitated TiC. However, no D was found at carbides smaller than 3 nm. Consequently they related the deep hydrogen trapping to defects at the broad semi-coherent TiC/matrix interface, being either carbon-vacancies or misfit dislocation cores. However, only limited interest has been paid to the trapping ability from a gaseous hydrogen-containing environment at elevated temperatures, while this being relevant for introduction during various production stages, e.g. heat treatments, galvanization, etc., and also in future hydrogen economy related applications.

In order to address this knowledge gap, this study focuses on the hydrogen trapping effect from a gaseous hydrogen containing environment at elevated temperature. In contrast to previous studies [29-32, 43], tempering was performed in a controlled dilute gaseous hydrogen atmosphere. To evaluate the effect of the undissolved carbides, two Fe-C-Ti alloys, differing in carbon and titanium content, were studied. Improved insight in the hydrogen trapping was obtained via combination of

experimental evaluation of the hydrogen interactions by TDS and melt extraction, together with detailed microstructural analysis and thermodynamical calculations.

Table 1: overview of different trapping sites and corresponding binding energy and density related to precipitated TiC, as reported in [34]

Trap	Trapping site	Binding energy (kJ/mol)	Trap density (mol/mm³)
1	Coherent interface	20-28	$4 \times 10^{-9} – 10^{-6}$
2	Carbon-vacancy at (semi-)coherent $(001)_{Fe}/(001)_{TiC}$ interface	55-60	$1\text{-}6 \times 10^{-9}$
3	Carbon-vacancy at incoherent $(110)_{Fe}/(001)_{TiC}$ interface	71-81	$5 \times 10^{-10} – 2 \times 10^{-9}$
4	Bulk carbon-vacancy	93-104	$3 \times 10^{-10} – 5 \times 10^{-10}$

Materials and Methods

Two different generic Fe-C-Ti materials were used in this study, for which the composition is given in Table 2. The steels were laboratory cast in a Pfeiffer VSG100 incremental vacuum melting and casting unit under an argon gas atmosphere and subsequently hot and cold rolled to a final thickness of 1mm. The cold rolled materials were subjected to a quench and temper treatment, in order to obtain a martensitic matrix containing titanium carbides. Austenitization was performed at 1250 °C in an air resistance furnace, followed by quenching in brine. According to the solubility product of the stoichiometric TiC [44], this corresponded to a dissolved carbon and titanium content of around 0.060 wt% and 0.238 wt%, respectively. Hence, a considerable, but different, amount of undissolved carbides was present in both Ti-containing alloys.

Table 2: Chemical composition of the materials, given in wt%

	C	Ti	V	Al	N	impurities
Fe-C-Ti (A)	0.202	0.740	0	0.02-0.03	0.0015-0.0020	0.0005-0.0010 S 0.0010-0.0020 P
Fe-C-Ti (B)	0.313	1.340	0	0.02-0.03	0.0015-0.0020	0.0005-0.0010 S 0.0010-0.0020 P

Tempering was performed at 600°C for 1h, in a tube furnace, either in air or in a hydrogen containing atmosphere at ambient pressure. Consequently, gaseous hydrogen charging could be performed simultaneous with tempering. All samples were discs with a diameter of 2 cm, punched from the as-quenched (asQ) plate. Grinding of the sample with #500 SiC paper allowed the removal of the oxide layer and similar surface roughness for all samples. In order to have good control over the temperature, the sample was positioned in the furnace by a thermocouple. A schematic visualization of the used set-up is shown in Figure 1. In case of hydrogen charging, the furnace was flushed with formier gas (containing 5% H_2 and 95% N_2) before insertion of the sample and a constant flux of approximately 50 l/h of formier gas was applied during tempering in order to maintain the atmosphere. Similarly for tempering in air, a flux of 50 l/h of air was blown through the furnace. After tempering the samples were quenched in water and immediately tested to minimize hydrogen effusion.

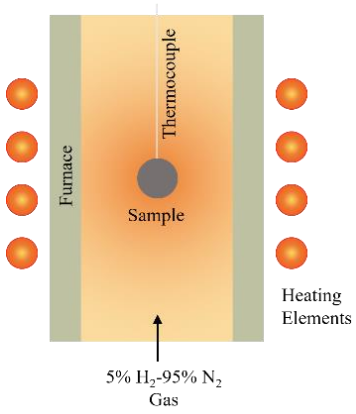

Figure 1: Schematic illustration of the set-up for gaseous charging at high temperature.

Characterization of the hydrogen/microstructure interactions was performed by hot extraction and TDS measurements using a Galileo G8 setup. During hot extraction measurements, the samples were subjected to a constant temperature of 950°C for 10 min and the desorbed hydrogen is transported via a N_2 flow to a TCD detector, allowing determination of the total hydrogen content of the samples. On the other hand, during TDS the samples were subjected to a constant heating rate (600 °C/h, 900°C/h, and 1200°C/h) and the hydrogen desorption rate was measured. In this case, the hydrogen desorbed is transported via a N_2 flow to a mass spectrometer, allowing the measurement of hydrogen per cycle of around 1.7 seconds.

Microstructural characterization was performed by scanning electron microscopy (SEM) together with energy dispersive X-ray (EDX) analysis. Etching with Nital 10% was done in order to reveal the martensitic matrix and TiC. However, in order to evaluate the carbide distributions, polished (unetched) samples were investigated. For each sample 15 images were taken, all at the same magnification. Based on the color contrast between matrix and precipitate, ImageJ was able to identify the carbides as particles. As such, area fractions of the precipitates could be obtained and the length of the major and minor axis of the fitted ellipses was used as an indication for the carbide sizes. Additionally, transmission electron microscopy (TEM) analysis was performed in order to study the small carbides. Thin foil samples for TEM observation are prepared by mechanical grinding and polishing the sample to a thickness of around 100 µm. Discs with a diameter of 3 mm are cut from the slice and are thinned in the central region by electropolishing using a twin jet method and a mixture of perchloric acid (4%) and acetic acid as electrolyte.

Results and Discussion

Microstructural analysis of the Fe-C-Ti alloys by SEM and EDX indicated that both materials had a tempered martensitic matrix containing many relatively large titanium carbides, as can be seen from Figure 2. These large carbides can be considered as the undissolved carbides since the precipitated carbides would be too small for observation via SEM. Moreover, the undissolved carbides appeared to be present in different shapes, i.e. elongated particles as well as round and square particles could be observed. The carbide shape is determined by the interfacial energy, and hence depends both on the matrix in which they are formed and the dimensions. Generally, disc-like particles are associated to TiC precipitated in a ferritic (BCC) matrix following the Baker-Nutting orientation relationship (OR) [45]. On the other hand, particles nucleated in the austenitic (FCC) matrix are reported to have both spherical and cuboidal shapes due to the cube-on-cube OR [46, 47]. Additionally, it has been reported that precipitates formed during the isothermal austenite to ferrite transformation, tend to adopt the Baker-Nutting OR and the corresponding disc shape while they are formed along the moving austenite/ferrite interface. However, they are typically distributed in a band-type fashion [47-51].

Consequently, the undissolved carbides in the Fe-C-Ti alloys probably originated from nucleation in the austenitic phase, together with interphase precipitation. The precipitated carbides on the other hand were much smaller and hence could only be visualized by TEM. While mainly disc-shaped carbides were observed, some round particles could be found as well. An example is given in Figure 3.

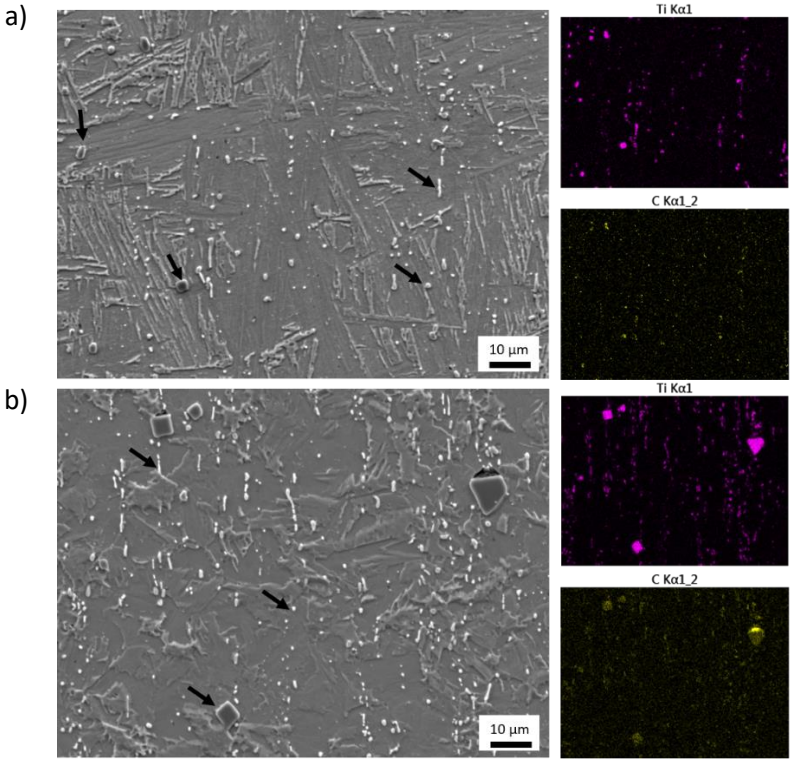

Figure 2: SEM images of the Q&T Fe-C-Ti (a) alloy A and (b) alloy B with the corresponding EDX elemental maps. Some TiC particles are indicated by black arrows

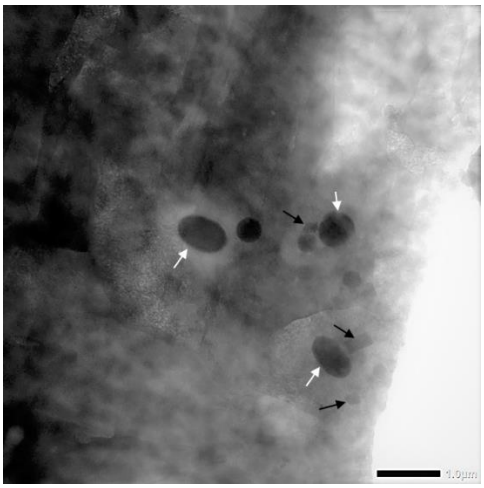

Figure 3: TEM image of the Q&T Fe-C-Ti alloy B, white arrows indicate undissolved TiC while black indicate precipitated.

Considering the similar austenitization temperature and tempering treatment of both alloys, a similar amount of carbon (and correspondingly titanium) should have dissolved during austenitization, leading to a similar amount, shapes and sizes of precipitated carbides, while a distinctly different amount of undissolved carbides could be expected. Therefore, focus lays on the SEM characterization and ImageJ analysis of the SEM images was performed to estimate the undissolved TiC area fraction together with the corresponding carbide size distribution. As expected, a higher area fraction was found for alloy B (2.74 ± 0.55 %) than for alloy A (1.63 ± 0.46%). The resulting histograms of the carbide sizes (both major

and minor axis) are shown in Figure 4. It appears that alloy B contained a higher fraction of large carbides while alloy A contained a higher fraction of smaller precipitates.

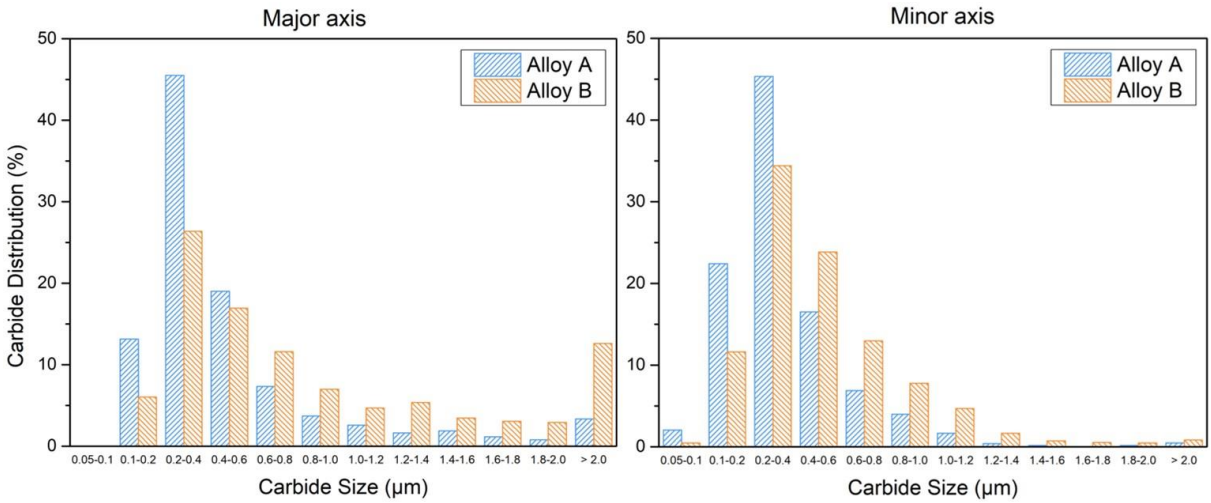

Figure 4: Histogram of the carbide sizes for the Q&T Fe-C-Ti alloy A and B, based on the ImageJ analysis of SEM images.

The hot extraction results, given in Figure 5, of the samples tempered in air versus tempering in hydrogen showed a strong increase of the hydrogen content after tempering in the hydrogen containing atmosphere. Hence, a considerable amount of hydrogen was introduced from the gaseous environment during tempering, despite the very low hydrogen partial pressure. According to Sievert's law and based on the results from Hirth [52, 53], the amount of hydrogen that could be absorbed by the iron lattice from a partial pressure of 0.05 bar at 600°C is around 0.145 wppm, which is considerably lower than the observed amount of hydrogen. Hence, the additional hydrogen introduced could be related to hydrogen trapped by the titanium carbides. Moreover, a significantly higher amount of hydrogen was introduced in alloy B than in alloy A, which already indicated that the undissolved carbides were mainly responsible for trapping as they were more frequently present in alloy B. However, it must be noted that a minor contribution of the precipitated, i.e. smaller, carbides could not be excluded.

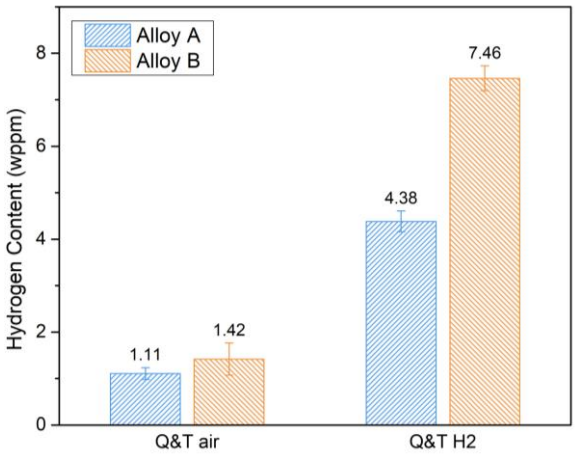

Figure 5: Hydrogen content as determined by hot extraction at 950°C of the Fe-C-Ti alloy A and B after tempering in air or in a hydrogen containing atmosphere.

Analysis of the trapping sites was done by TDS. Figure 6 shows the TDS spectra of the gaseously hydrogen charged samples. A high temperature peak between 500°C and 900°C appeared for both alloys, indicating very strong trapping. This nicely agrees with the results from Wei et al. [29-32] and Perez Escobar et al. [43], who observed a TDS peak in a similar temperature range for titanium-carbide

containing steels and they related this peak to hydrogen trapping by the carbon-vacancies in the bulk of the undissolved TiC or at the incoherent interfaces. Considering the same peak temperature range, similar activation energies could be expected for alloy A and B, despite the differences in carbide size distribution. However, large deviations on peak shape and maximum temperature were observed for different samples and different heating rates. Consequently, no consistent deconvolution of the desorption peak into multiple peaks to account for different trapping sites could be obtained and hence the method of Choo and Lee [54] based on the Kissinger equation [55] for determination of the de-trapping activation energy could not give reliable results in the present case. This is in contrast to the findings of Perez Escobar et al. [43], who studied hydrogen trapping in a titanium containing steel tempered at various temperatures under a 1 bar pure H_2 atmosphere. They also observed a high temperature peak, which after deconvolution into Gaussian peaks revealed the presence of up to three sub-peaks. Application of the Choo-Lee method resulted in an activation energy of around 135 kJ/mol for the first peak and around 150 kJ/mol for both the second and third peak. The existence of two different peaks with similar activation energy was linked to a difference in pre-exponential factor in the Kissinger equation. However no physical interpretation was given for this effect, nor was it linked to any microstructural effect. Additionally, tempering above 600°C resulted in the disappearance of the first peak but no significant change upon tempering was reported for the second and third peak was reported. They observed a slight increase in carbide size with increasing annealing temperature, but no link was made between the microstructural changes and the variations in TDS peaks. Rather, all peaks were simply related to trapping by carbon-vacancies in the bulk of the titanium carbides. Wei and Tsuzaki [29-32], on the other hand, reported a single high temperature peak but they observed a wide range of activation energies from 68 kJ/mol to 137 kJ/mol for this peak, depending on material composition, austenitization temperature, and tempering/charging temperature. However, no clear correlation between carbide size or structure and the activation energies was reported as well. Consequently, ambiguity still exists upon number of trapping sites related to the carbon-vacancies and influence of carbide sizes and structures.

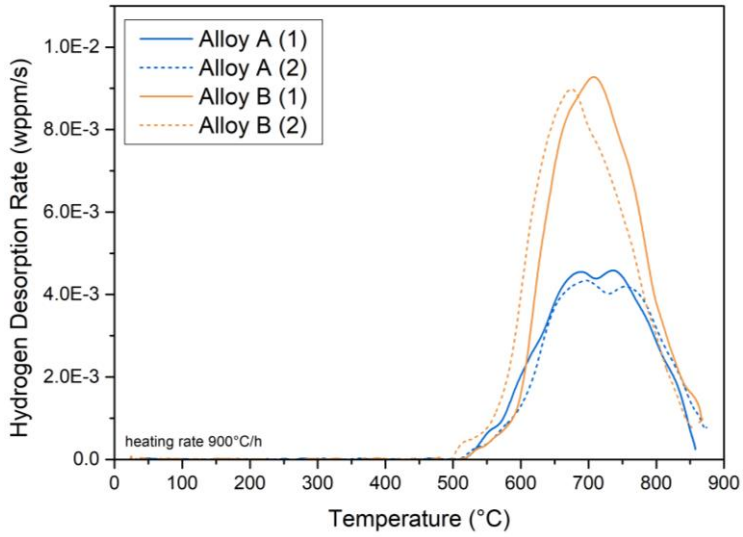

Figure 6: TDS spectra of Fe-C-Ti alloys A and B tempered for 1h at 600°C in the gaseous hydrogen containing environment. Measurements of two different samples are shown for each condition, one as solid and one as dashed line, visualizing experimental variations due to varying carbide density in the microstructure.

Theoretical calculations performed by Di Stefano et al. [33] indicated the presence of only two sites with strong binding (E_B higher than 60 kJ/mol), i.e. the carbon-vacancies at the interface (E_B= 87 kJ/mol) and bulk carbon-vacancies (E_B= 105 kJ/mol). While DFT studies performed by Hammer et al. [56] indicated a lowering of the binding energy upon the addition of Mo and V, no change in binding

energy due to variations in carbon-vacancy concentration have been reported [33]. This would mean that maximal two trapping sites with different binding energy are presently active in the titanium carbides at the elevated temperature. Additionally, due to the large volume of the carbides, the bulk carbon-vacancy concentration is expected to be much higher than the interface carbon-vacancies, resulting in one main hydrogen binding energy site. However, a much higher activation energy for hydrogen to leave the carbon-vacancy was found when it is isolated than in the case of connected carbon-vacancies, i.e. 170 kJ/mol vs 114 kJ/mol, respectively. This is consistent with the experimental study by Nguyen et al. [57], revealing easy hydrogen diffusion through sub-stoichiometric TiC containing connected vacancies while TiC without a well-developed carbon-vacancy network showed very difficult hydrogen diffusion. Consequently, detrapping of hydrogen from a bulk carbon-vacancy will be influenced by the carbon-vacancy concentration and ordering. Moreover, desorption of hydrogen not only requires simple detrapping from the carbon-vacancy but also diffusion throughout the titanium carbide. Energy schematics based on the DFT calculations of Di Stefano et al. [33] are shown in Figure 7. Clearly, desorption of hydrogen is strongly affected by the number of jumps throughout the carbide, i.e. the carbide size, as well as carbide structure and vacancy concentration. Consequently, a distribution of carbide sizes and variances in carbon-vacancy concentration/network formation might result in an irregular desorption peak in the TDS spectrum, looking similar to multicomponent trapping. Therefore, the observed discrepancies in the TDS spectra could be due to small material and processing variations leading to differences in carbide size distributions and structures for different samples.

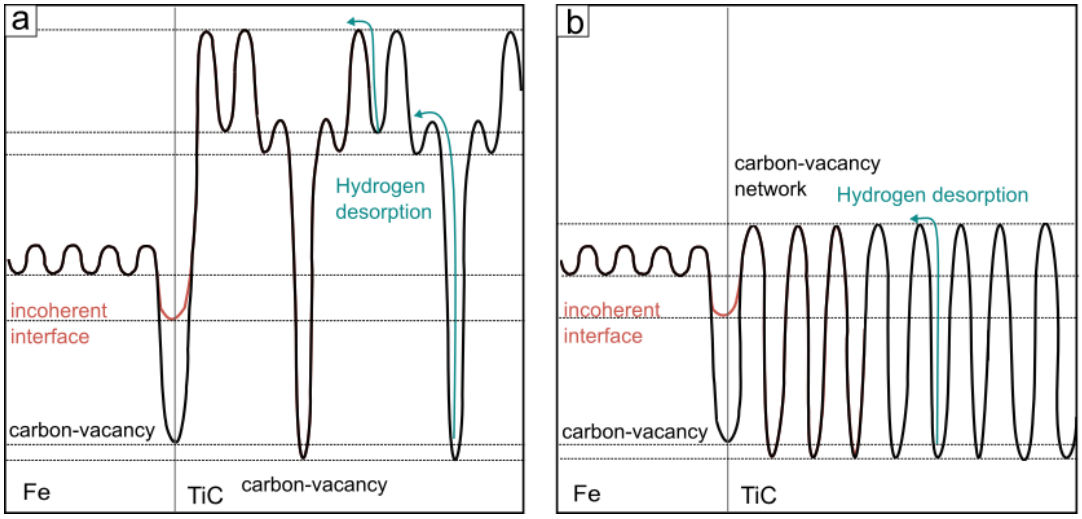

Figure 7: Schematic drawing of the energy profiles experienced by hydrogen atoms in titanium carbides containing (a) isolated vacancies and (b) a connected carbon-vacancy network. (Based on the work of Di Stefano et al. [33])

Consequently, literature data allowed clearly linking the observed hydrogen uptake and trapping at elevated temperatures to the carbon-vacancies in the titanium carbides based on both DFT calculations and experimental data. Subsequently, Factsage was used to calculate an estimated equilibrium amount of carbon-vacancies in the TiC for the different steel compositions, which is shown in Figure 8. It can be seen from this figure that the carbon-vacancy concentration in alloy A continuously decreased towards zero with decreasing temperature, while for alloy B it decreased to a constant value of around 5.8E-3 mol/cm^3_{TiC}. This difference could be related to the off-stoichiometric composition of the alloys. Alloy A contained an excess of carbon, while alloy B was depleted in carbon. Hence, alloy B did not contain sufficient carbon to form TiC completely free of vacancies and thus the minimum amount of vacancies present in this alloy was determined by the carbon deficit rather than by the vacancy formation energy. Multiplication of the equilibrium carbon-vacancy concentration at 600°C with the carbide content in the sample, as predicted by Factsage, allowed estimating the amount

of available trapping sites and hence the maximum possible hydrogen content. For alloy B, this resulted a maximum hydrogen solubility of 19.44 wppm. However, for alloy A a maximum solubility of only 3.85 wppm hydrogen was found by this approach. This discrepancy could be related to the dependence of the carbon-vacancy concentration on the carbide precipitation temperature. Indeed, the undissolved carbides were formed at a higher temperature than the precipitated carbides. Consequently, these carbides should have a much higher vacancy concentration than predicted for 600°C. A decrease of the carbon-vacancy concentration towards the 600°C equilibrium value would require a considerable transport of carbon within the carbide. However, the energy barriers for carbon diffusion in the titanium carbides are reported to be very large [33, 58-60]. Therefore, the vacancies in the undissolved carbides can be considered as "frozen in" and no changes occurred in the carbon-vacancy content of the undissolved carbides during the tempering for 1h at 600°C. The resulting total amount of carbon-vacancies could thus be estimated by using the equilibrium concentration at 600°C only for the precipitated carbides and the equilibrium concentration at the austenitization temperature for the undissolved carbides. This resulted in a maximum hydrogen solubility of 13.69 wppm for alloy A, with 12.61 wppm in the undissolved and 1.07 wppm in the precipitated carbides. Using the same approach for alloy B, a total solubility of 30.26 wppm hydrogen was obtained, for which 26.79 wppm in the undissolved and 3.47 wppm in the precipitated carbides. Hence, the undissolved carbides were confirmed to be the main trapping sites providers while the precipitated carbides might only make a small contribution.

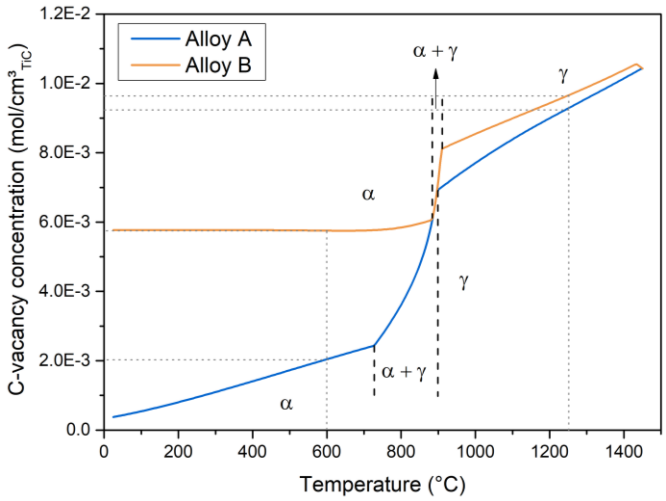

Figure 8: Equilibrium C-vacancy concentration in TiC as a function of temperature calculated by Factsage for both Fe-C-Ti alloy compositions. The different regions of the matrix phases are indicated as well. Higher C-Vacancy concentrations can be expected for the undissolved carbides (T=1250°C) than for the precipitated carbides (T=600°C).

In the case of one binding energy for all carbon-vacancy related trapping sites, one can estimate the trap binding energy assuming saturation has been reached and considering local equilibrium between the interstitial lattice sites and the carbon-vacancies inside the TiC, as is represented by the equation given below:

$$H_L + \mathcal{V}_T \rightleftharpoons \mathcal{V}_L + H_T \qquad [1]$$

With H_L the hydrogen atom in interstitial lattice position, $\mathcal{V}_T$ a vacant trapping site, $\mathcal{V}_L$ a vacant lattice site and H_T hydrogen in the trapping site. Consequently, at equilibrium the different concentrations are given by equation 2.

$$\frac{c_T*(N_L-c_L)}{c_L*(N_T-c_T)} = A * \exp\left(-\frac{E_B}{RT}\right) \qquad [2]$$

With c_L and c_T the concentration of lattice and trapped hydrogen, respectively, N_L the concentration of interstitial lattice sites, and N_T the trap density, all in mol/m³, E_B the binding energy in J/mol, A the pre-exponential factor (related to the entropic contribution), R the ideal gas constant and T the temperature in K. For N_T, the above calculated values for the concentration of carbon-vacancies could be used. It must be noted that by tempering in a hydrogen-containing environment TiC precipitation could be affected by the presence of hydrogen, possibly resulting in a higher concentration of carbon-vacancies. However, not the precipitated carbides formed upon tempering but the undissolved carbides were found to be of major importance. These carbides were already present before start of hydrogen charging (and tempering). Moreover, change of carbon-vacancy concentration would require long range migration of C through the carbides which is characterized by very high activation energies (235 kJ/mol-396 kJ/mol) [33, 58-60], whereas hydrogen diffusion throughout the TiC is much easier (26 kJ/mol-45kJ/mol [33,61] for interstitial diffusion, 87 kJ/mol for vacancy-mediated diffusion [32]). Therefore, it is reasonable to assume that presence of hydrogen does not significantly affect the bulk carbon-vacancy concentration. The trapped hydrogen concentration c_T was determined by the hot extraction measurements while the lattice hydrogen concentration was assumed to be equal to the equilibrium concentration induced in the steel at 600°C for a hydrogen partial pressure of 0.05 bar, based on Sievert's law. For A and N_L values were taken from literature. Based on literature data [31, 34, 39, 62, 63], the pre-exponential factor was set to 1. Various values have been reported for the concentration interstitial lattice sites. Therefore, E_B was calculated for some of the different reported values of N_L to evaluate its effect on the obtained value of E_B. An overview of the different parameters used in this calculation is given in Table 3 and the resulting E_B values are summarized in Table 4.

As a result, binding energies ranging between 80 kJ/mol and 90 kJ/mol were obtained depending on the used value for N_L. These values are in the range obtained by Wei and Tsuzaki [29-32] and are also in relative good agreement with the DFT calculated values reported in literature [33, 64]. Consequently, the estimated binding energies nicely agree with the binding to the bulk carbon-vacancies in TiC. The increase in number of trapping sites present due to addition of the precipitated carbides resulted in only very small decrease of the value obtained for E_B. Consequently, minor contribution of the precipitated carbides could still not be fully excluded. More importantly, very similar binding energies were found for alloy A and B, in perfect agreement with the TDS measurements. Consequently, the binding energy of hydrogen to the carbon-vacancies could be assumed to be very similar in both alloys, despite the different carbide sizes. However, it must be noted that due to the high barriers for hydrogen migration inside the carbide [33, 65], uncertainty remains on the distribution of hydrogen within the TiC which might impact the validity of the local equilibrium approach. Therefore, tempering for longer time (21h) in the hydrogen atmosphere was done for both alloys. This resulted in a slight increase of the H content to 4.83 ± 0.31 wppm and 7.79 ± 0.34 wppm for alloy A and B, respectively. However, the corresponding impact on the binding energy values was negligible (maximum decrease of 1.1 kJ/mol). It must be noted that the above analysis is only valid in the case of one binding energy site, i.e. the bulk carbon-vacancy in analogy to the theoretical work by Di Stefano et al. [33]. Considering the large volume of the carbides, it is reasonable to assume bulk carbon-vacancies are much more abundant than the carbon-vacancies at the interface, and hence trapping by the interface may be neglected.

Table 3: Concentration values used in calculation of binding energy (given in mol/m³).

Parameter	concentration	source
c_L	1.13	[52]
N_L	873464	[31]
	140997.4	[63]
	204100	[62]
	833000	[34, 39]
c_T	34.22	Hot extraction value for alloy A
	58.28	Hot extraction value for alloy B
N_T	98.52	Carbon-vacancy concentration in undissolved carbides in alloy A as determined by Factsage
	106.9	Carbon-vacancy concentration in undissolved and precipitated carbides in alloy A as determined by Factsage
	209.28	Carbon-vacancy concentration in undissolved carbides in alloy B as determined by Factsage
	236.40	Carbon-vacancy concentration in undissolved and precipitated carbides in alloy B as determined by Factsage

Table 4: Calculated binding energies (in kJ/mol) corresponding to different interstitial lattice positions as reported in literature.

	Undissolved	Undissolved & precipitated	N_L
Alloy A	93.8	92.9	[31]
	80.6	97.7	[63]
	83.2	82.4	[62]
	93.5	92.5	[34, 39]
Alloy B	91.5	90.3	[31]
	78.2	77.0	[63]
	80.9	79.7	[62]
	91.1	89.9	[34, 39]

Conclusions

In this study, generic Fe-C-Ti alloys were subjected to a quench and temper treatment where the tempering environment was either air or a 5% H_2-95% N_2 mixture. As such the hydrogen uptake due to trapping at elevated temperatures could be evaluated. It was shown that the Fe-C-Ti alloys were able to trap considerable amounts of hydrogen, resulting in a high temperature peak in the TDS spectrum, which was related to the strong binding of hydrogen to carbon-vacancies inside the titanium carbides. The main contribution was attributed to the undissolved, incoherent carbides, which was related to their high carbon-vacancy concentration as well as their significant volume. The small carbides precipitated during tempering did not contribute to the hydrogen trapping or only to a very limited extent. Consequently, the (semi-)coherent interface and low carbon-vacancy density made the small nucleating carbides unsuitable for hydrogen uptake at high temperatures.

Due to variations in desorption peak shapes and positions no reliable activation energy could be obtained from the TDS spectra. However, a theoretical binding energy could be determined based on the trapped hydrogen content and assuming equilibrium between hydrogen in lattice and in trapping

sites. For both alloys, very similar binding energy values of around 85 kJ/mol were obtained, independent of the undissolved carbide size. Further investigations should confirm these calculations.

Acknowledgements

The authors would like to thank Elien Wallaert for the TEM investigations, Vincent Cnockaert and Olivier Vergote for the development and optimization of the gaseous charging set-up, as well as dr. Lotte De Vos for her help with the Factsage calculations. Additionally, they would like to thank Simon Spoelders as he performed considerable part of the experiments on the Fe-C-Ti alloy B in the context of his master dissertation. Furthermore, the authors wish to thank the doctoral and senior postdoctoral fellowship of the Research Foundation – Flanders (FWO) via grant 11F6520N and 12ZO420N and the Special Research Fund (BOF), UGent (grants BOF15/BAS/062, OF/GOA/026, and BOF20/BAS/121) for support.

Conflict of Interest

No potential conflict of interest is reported by the authors.

References

[1] Depover T, Pérez Escobar D, Wallaert E, Zermout Z, Verbeken K. Effect of hydrogen charging on the mechanical properties of advanced high strength steels. International Journal of Hydrogen Energy. 2014;39:4647-56.
[2] Depover T, Wallaert E, Verbeken K. On the synergy of diffusible hydrogen content and hydrogen diffusivity in the mechanical degradation of laboratory cast Fe-C alloys. Materials Science and Engineering: A. 2016;664:195-205.
[3] Meda US, Bhat N, Pandey A, Subramanya KN, Lourdu Antony Raj MA. Challenges associated with hydrogen storage systems due to the hydrogen embrittlement of high strength steels. International Journal of Hydrogen Energy. 2023.
[4] Laureys A, Depraetere R, Cauwels M, Depover T, Hertelé S, Verbeken K. Use of existing steel pipeline infrastructure for gaseous hydrogen storage and transport: A review of factors affecting hydrogen induced degradation. Journal of Natural Gas Science and Engineering. 2022;101:104534.
[5] Wang H, Tong Z, Zhou G, Zhang C, Zhou H, Wang Y, et al. Research and demonstration on hydrogen compatibility of pipelines: a review of current status and challenges. International Journal of Hydrogen Energy. 2022;47:28585-604.
[6] Wu X, Zhang H, Yang M, Jia W, Qiu Y, Lan L. From the perspective of new technology of blending hydrogen into natural gas pipelines transmission: Mechanism, experimental study, and suggestions for further work of hydrogen embrittlement in high-strength pipeline steels. International Journal of Hydrogen Energy. 2022;47:8071-90.
[7] Briottet L, Moro I, Lemoine P. Quantifying the hydrogen embrittlement of pipeline steels for safety considerations. International Journal of Hydrogen Energy. 2012;37:17616-23.
[8] Zhang P, Laleh M, Hughes AE, Marceau RKW, Hilditch T, Tan MY. A systematic study on the influence of electrochemical charging conditions on the hydrogen embrittlement behaviour of a pipeline steel. International Journal of Hydrogen Energy. 2023.
[9] Zhou C, Ye B, Song Y, Cui T, Xu P, Zhang L. Effects of internal hydrogen and surface-absorbed hydrogen on the hydrogen embrittlement of X80 pipeline steel. International Journal of Hydrogen Energy. 2019;44:22547-58.
[10] Depraetere R, De Waele W, Cauwels M, Depover T, Verbeken K, Boone M, et al. Influence of stress triaxiality on hydrogen assisted ductile damage in an X70 pipeline steel. Materials Science and Engineering: A. 2023;864:144549.
[11] Cauwels M, Depraetere R, De Waele W, Hertelé S, Depover T, Verbeken K. Influence of electrochemical hydrogenation parameters on microstructures prone to hydrogen-induced cracking. Journal of Natural Gas Science and Engineering. 2022;101:104533.
[12] Vander Vennet S, Leitner S, Razumovskiy V, Ecker W, Depover T, Verbeken K. Mechanical load induced hydrogen charging of retained austenite in quenching and partitioning (Q&P) steel. International Journal of Hydrogen Energy. 2023;48:2428-41.

[13] Okayasu M, Fujiwara T. Hydrogen embrittlement characteristics of hot-stamped 22MnB5 steel. International Journal of Hydrogen Energy. 2021;46:19657-69.
[14] Grange RA, Hribal CR, Porter LF. Hardness of tempered martensite in carbon and low-alloy steels. Metallurgical Transactions A. 1977;8:1775-85.
[15] Speich GR, Leslie WC. Tempering of Steel. Metallurgical and Materials Transactions B. 1972;3:1043-54.
[16] Depover T, Verbeken K. The effect of TiC on the hydrogen induced ductility loss and trapping behavior of Fe-C-Ti alloys. Corrosion Science. 2016;112:308-26.
[17] Nagao A, Martin ML, Dadfarnia M, Sofronis P, Robertson IM. The effect of nanosized (Ti,Mo)C precipitates on hydrogen embrittlement of tempered lath martensitic steel. Acta Materialia. 2014;74:244-54.
[18] Kim H-J, Jeon S-H, Yang W-S, Yoo B-G, Chung Y-D, Ha H-Y, et al. Effects of titanium content on hydrogen embrittlement susceptibility of hot-stamped boron steels. Journal of Alloys and Compounds. 2018;735:2067-80.
[19] Depover T, Laureys A, Perez Escobar D, Van den Eeckhout E, Wallaert E, Verbeken K. Understanding the Interaction between a Steel Microstructure and Hydrogen. Materials (Basel). 2018;11.
[20] Depover T, Verbeken K. The detrimental effect of hydrogen at dislocations on the hydrogen embrittlement susceptibility of Fe-C-X alloys: An experimental proof of the HELP mechanism. International Journal of Hydrogen Energy. 2018;43:3050-61.
[21] Laureys A, Claeys L, De Seranno T, Depover T, Van den Eeckhout E, Petrov R, et al. The role of titanium and vanadium based precipitates on hydrogen induced degradation of ferritic materials. Materials Characterization. 2018;144:22-34.
[22] Pressouyre GM, Bernstein IM. A quantitative analysis of hydrogen trapping. Metallurgical Transactions A. 1978;9:1571-80.
[23] Devanathan MAV, Stachurski Z, Tompkins FC. The adsorption and diffusion of electrolytic hydrogen in palladium. Proceedings of the Royal Society of London Series A Mathematical and Physical Sciences. 1962;270:90-102.
[24] Asaoka T, Lapasset G, Aucouturier M, Lacombe P. Observation of hydrogen trapping in Fe-0.15wt% Ti alloy by high resolution autoradiography. Corrosion. 1978;34:39-.
[25] Stevens MF, Bernstein IM. Microstructural trapping effects on hydrogen induced cracking of a microalloyed steel. Metallurgical Transactions A. 1989;20A:909-19.
[26] Valentini R, Solina A, Matera S, De Gregorio P. Influence of Titanium and Carbon Contents on the Hydrogen Trapping of Microalloyed Steels. Metallurgical and Materials Transactions A. 1996;27A:3773.
[27] Lee HG, Lee J-Y. Hydrogen Trapping by TiC particles in Iron. Acta Metallurgica. 1984;32:131-6.
[28] Lee SM, Lee J-Y. The effect of the interface character of TiC particles on hydrogen trapping in steel. Acta Metallurgica. 1987;35:2695-700.
[29] Wei FG, Hara T, Tsuchida T, Tsuzaki K. Hydrogen Trapping in Quenched and Tempered 0.42C-0.30Ti Steel Containing Bimodally Dispersed TiC Particles. ISIJ International. 2003;43:539-247.
[30] Wei FG, Hara T, Tsuzaki K. Precise determination of the activation energy for desorption of hydrogen in two Ti-added steels by a single thermal-desorption spectrum. Metallurgical and Materials Transactions B. 2004;35:587-97.
[31] Wei FG, Tsuzaki K. Hydrogen absorption of incoherent TiC particles in Iron from Environment at High Temperatures. Metallurgical and Materials Transactions A. 2004;35:3155-63.
[32] Wei FG, Tsuzaki K. Quantitative analysis on hydrogen trapping of TiC particles in steel. Metallurgical and Materials Transactions A. 2006;37:331-53.
[33] Di Stefano D, Nazarov R, Hickel T, Neugebauer J, Mrovec M, Elsässer C. First-principles investigation of hydrogen interaction with TiC precipitates inα-Fe. Physical Review B. 2016;93:184108.
[34] Drexler A, Depover T, Verbeken K, Ecker W. Model-based interpretation of thermal desorption spectra of Fe-C-Ti alloys. Journal of Alloys and Compounds. 2019;789:647-57.
[35] Takahashi J, Kawakami K, Kobayashi Y, Tarui T. The first direct observation of hydrogen trapping sites in TiC precipitation-hardening steel through atom probe tomography. Scripta Materialia. 2010;63:261-4.
[36] Depover T, Monbaliu O, Wallaert E, Verbeken K. Effect of Ti, Mo and Cr based precipitates on the hydrogen trapping and embrittlement of Fe–C–X Q&T alloys. International Journal of Hydrogen Energy. 2015;40:16977-84.
[37] Van den Eeckhout E, Depover T, Verbeken K. The Effect of Microstructural Characteristics on the Hydrogen Permeation Transient in Quenched and Tempered Martensitic Alloys. Metals. 2018;8:779.
[38] Lin Y-C, McCarroll IE, Lin Y-T, Chung W-C, Cairney JM, Yen H-W. Hydrogen trapping and desorption of dual precipitates in tempered low-carbon martensitic steel. Acta Materialia. 2020;196:516-27.

[39] Drexler A, Depover T, Leitner S, Verbeken K, Ecker W. Microstructural based hydrogen diffusion and trapping models applied to Fe–C X alloys. Journal of Alloys and Compounds. 2020;826:154057.
[40] Takahashi J, Kawakami K, Kobayashi Y. Origin of hydrogen trapping site in vanadium carbide precipitation strengthening steel. Acta Materialia. 2018;153:193-204.
[41] Chen Y-S, Lu H, Liang J, Rosenthal A, Liu H, Sneddon G, et al. Observation of hydrogen trapping at dislocations, grain boundaries, and precipitates. Science. 2020;367:171-5.
[42] Chen Y-S, Haley D, Gerstl SSA, London AJ, Sweeney F, Wepf RA, et al. Direct observation of individual hydrogen atoms at trapping sites in a ferritic steel. Science. 2017;355:1196-9.
[43] Pérez Escobar D, Wallaert E, Duprez L, Atrens A, Verbeken K. Thermal desorption spectroscopy study of the interaction of hydrogen with TiC precipitates. Metals and Materials International. 2013;19:741-8.
[44] Gorni AA. Steel forming and heat treating handbook. São Vicente, Brazil2011.
[45] Wei F-G, Hara T, Tsuzaki K. High-resolution transmission electron microscopy study of crystallography and morphology of TiC precipitates in tempered steel. Philosophical Magazine. 2004;84:1735-51.
[46] Wang Z, Sun X, Yang Z, Yong Q, Zhang C, Li Z, et al. Carbide precipitation in austenite of a Ti–Mo-containing low-carbon steel during stress relaxation. Materials Science and Engineering: A. 2013;573:84-91.
[47] Yen HW, Chen CY, Wang TY, Huang CY, Yang JR. Orientation relationship transition of nanometre sized interphase precipitated TiC carbides in Ti bearing steel. Materials Science and Technology. 2010;26:421-30.
[48] Davenport AT, Honeycombe RWK, Cottrell AH. Precipitation of carbides at γ–α boundaries in alloy steels. Proceedings of the Royal Society of London A Mathematical and Physical Sciences. 1971;322:191-205.
[49] Honeycombe RWK, Mehl RF. Transformation from austenite in alloy steels. Metallurgical Transactions A. 1976;7:915-36.
[50] Yen H-W, Chen P-Y, Huang C-Y, Yang J-R. Interphase precipitation of nanometer-sized carbides in a titanium–molybdenum-bearing low-carbon steel. Acta Materialia. 2011;59:6264-74.
[51] Dong H, Chen H, Riyahi khorasgani A, Zhang B, Zhang Y, Wang Z, et al. Revealing the influence of Mo addition on interphase precipitation in Ti-bearing low carbon steels. Acta Materialia. 2022;223:117475.
[52] Hirth JP. Effects of Hydrogen on the Properties of Iron and Steel. Metallurgical Transactions A. 1980;11:861-90.
[53] Nagumo M. Fundamentals of Hydrogen Embrittlement: Springer, Singapore; 2016.
[54] Choo WY, Lee J-Y. Thermal analysis of trapped hydrogen in pure iron. Metallurgical Transactions A. 1982;13:135-40.
[55] Kissinger HE. Reaction Kinetics in Differential Thermal Analysis. Analytical Chemistry. 1957;29:1702-6.
[56] Hammer P, Scheiber D, Ecker W, Romaner L, Moitzi F, Galler M, et al. Atomistic Modelling of Hydrogen Trapping on Coherent and Semi-coherent Ti-based Carbonitrides and Mixed-Metal Carbides in bcc Fe. In: Meseure K, editor. 4th International Conference on Metals Hydrogen. Ghent: Duprez, Lode;; 2022. p. L03.
[57] Nguyen J, Glandut N, Jaoul C, Lefort P. Hydrogen insertion in substoichiometric titanium carbide. International Journal of Hydrogen Energy. 2015;40:8562-70.
[58] Kohlstedt DL, Williams WS, Woodhouse JB. Chemical Diffusion in Titanium Carbide Crystals. Journal of Applied Physics. 1970;41:4476-84.
[59] Tsetseris L, Pantelides ST. Vacancies, interstitials and their complexes in titanium carbide. Acta Materialia. 2008;56:2864-71.
[60] van Loo FJJ, Bastin GF. On the diffusion of Carbon in Titanium Carbide. Metallurgical Transactions A. 1989;20A:403-11.
[61] Li Y, Zhang X, Wu T, Tang J, Deng L, Li W, et al. First-principles study on the dissolution and diffusion behavior of hydrogen in carbide precipitates. International Journal of Hydrogen Energy. 2021;46:22030-9.
[62] Drexler A, Vandewalle L, Depover T, Verbeken K, Domitner J. Critical verification of the Kissinger theory to evaluate thermal desorption spectra. International Journal of Hydrogen Energy. 2021;46:39590-606.
[63] Kirchheim R. Bulk Diffusion-Controlled Thermal Desorption Spectroscopy with Examples for Hydrogen in Iron. Metallurgical and Materials Transactions A. 2015;47:672-96.
[64] Kawakami K, Matsumiya T. Numerical analysis of hydrogen trap state by TiC and V4C3 in bcc-iron. ISIJ International. 2012;52:1693-7.
[65] Ding H, Fan X, Li C, Liu X, Jiang D, Wang C. First-principles study of hydrogen storage in non-stoichiometric TiCx. Journal of Alloys and Compounds. 2013;551:67-71.